Report

Current Biology

Convergent evolution of dim light vision in owls and deep-diving whales

Highlights:

- Convergent evolution of Q69R in the rod arrestin of owls and deep-diving whales
- Q69R occurs in the binding interface of rod arrestin and rhodopsin
- This mutation enhances sequestration of toxic all-trans retinal by rhodopsin
- Suggests a novel strategy for treating human blindness caused by all-trans retinal

Authors

Gianni M. Castiglione, Yan L.I. Chiu, Eduardo de A. Gutierrez, ..., Nihar Bhattacharyya, Ryan K. Schott, Belinda S.W. Chang

Correspondence

gianni.castiglione@vanderbilt.edu (G.M.C.), belinda.chang@utoronto.ca (B.S.W.C.)

In brief

Castiglione et al. identify the convergent evolution of a rare mutation in owls and deep-diving whales. These dim-light specialists also regularly encounter bright sunlight, creating elevated risk for blindness. This mutation enhances sequestration of toxic bright-light by-products, suggesting a novel clinical strategy for treating human blindness.

Castiglione et al., 2023, Current Biology *33*, 4733–4740
November 6, 2023
https://doi.org/10.1016/j.cub.2023.09.015

CellPress

Current Biology

CellPress

Report

Convergent evolution of dim light vision in owls and deep-diving whales

Gianni M. Castiglione,[1,2,3,4,5,10,11,13,*] Yan L.I. Chiu,[3] Eduardo de A. Gutierrez,[4] Alexander Van Nynatten,[3,6] Frances E. Hauser,[4,6] Matthew Preston,[3] Nihar Bhattacharyya,[3,7] Ryan K. Schott,[4,8,9] and Belinda S.W. Chang[3,4,12,*]

[1]Department of Biological Sciences, Vanderbilt University, Nashville, TN 37232, USA
[2]Department of Ophthalmology & Visual Sciences, Vanderbilt University, Nashville, TN 37232, USA
[3]Department of Cell & Systems Biology, University of Toronto, Toronto, ON M5S 3G5, Canada
[4]Department of Ecology & Evolutionary Biology, University of Toronto, Toronto, ON M5S 3B2, Canada
[5]Evolutionary Studies, Vanderbilt University, Nashville, TN 37235, USA
[6]Department of Biological Sciences, University of Toronto Scarborough, Toronto, ON M1C 1A4, Canada
[7]Institute of Ophthalmology, University College London, London EC1V 2PD, UK
[8]Department of Biology and Centre for Vision Research, York University, Toronto, ON M3J 1P3, Canada
[9]Department of Vertebrate Zoology, National Museum of Natural History, Smithsonian Institution, Washington, DC 20560, USA
[10]Present address: Department of Biological Sciences, Vanderbilt University, Nashville, TN, USA
[11]X (formerly Twitter): @giannicast
[12]X (formerly Twitter): @opsinlab
[13]Lead contact
*Correspondence: gianni.castiglione@vanderbilt.edu (G.M.C.), belinda.chang@utoronto.ca (B.S.W.C.)
https://doi.org/10.1016/j.cub.2023.09.015

SUMMARY

Animals with enhanced dim-light sensitivity are at higher risk of light-induced retinal degeneration when exposed to bright light conditions.[1–4] This trade-off is mediated by the rod photoreceptor sensory protein, rhodopsin (RHO), and its toxic vitamin A chromophore by-product, all-*trans* retinal.[5–8] Rod arrestin (Arr-1) binds to RHO and promotes sequestration of excess all-*trans* retinal,[9,10] which has recently been suggested as a protective mechanism against photoreceptor cell death.[2,11] We investigated Arr-1 evolution in animals at high risk of retinal damage due to periodic bright-light exposure of rod-dominated retinas. Here, we find the convergent evolution of enhanced Arr-1/RHO all-*trans*-retinal sequestration in owls and deep-diving whales. Statistical analyses reveal a parallel acceleration of Arr-1 evolutionary rates in these lineages, which is associated with the introduction of a rare Arr-1 mutation (Q69R) into the RHO-Arr-1 binding interface. Using *in vitro* assays, we find that this single mutation significantly enhances RHO-all-*trans*-retinal sequestration by ~30%. This functional convergence across 300 million years of evolutionary divergence suggests that Arr-1 and RHO may play an underappreciated role in the photoprotection of the eye, with potentially vast clinical significance.

RESULTS AND DISCUSSION

Arrestins are structurally dynamic signal transduction components that can function both dependently and independently of G protein signaling cascades.[12–14] Arrestin activation through binding interactions with G protein-coupled receptors (GPCRs) is a multimodal process that involves the phosphorylated receptor C-tail, and/or the transmembrane core; these interactions modulate the binding of the arrestin finger-loop (FL) domain to the intracellular cleft of the GPCR transmembrane core.[15–18] Non-visual arrestin beta 1 (ARRB1) and arrestin beta 2 (ARRB2) (also known as β-arrestins) recognize several hundred GPCRs, and similarly, cone arrestin (ARR3) also displays promiscuous binding but is likely regulated by co-expression with cone opsins within cone photoreceptors.[19,20] By contrast, rod photoreceptor arrestin (also known as arrestin-1 [Arr-1]; encoded by *SAG*) is exquisitely specific to the rod visual pigment rhodopsin (RHO),[20,21] which mediates dim-light vision through activation of G protein transducin (Gt)[22] (Figure 1A). Under dim-light conditions, RHO-Gt signaling is rapidly quenched following RHO phosphorylation and subsequent Arr-1 binding[11] (Figures 1A and 1B). During the onset of daylight conditions, massive concentrations of Arr-1 (~0.8mM) self-associated in the rod inner segment traffic to rod outer segments and are constitutively bound to RHO[11] (Figure 1C). Although Arr-1 mediated shutoff of excessive RHO-G_t signaling has been demonstrated as photoprotective under dim-light, bright-light damage in Arr-1 knockout mice is not blocked by removal of G_t.[23] Thus, the constitutive association of Arr-1 and RHO during daylight conditions has been theorized as a rod survival mechanism that is independent of excessive signaling.[2,11] Interestingly, an intrinsically photoprotective role has been proposed for RHO and Arr-1, comprising a functional trade-off that may have constrained the optimization of rod photosensitivity.[2,24]

RHO is required for light-induced retinal degeneration in mice, as is RPE65—a visual cycle enzyme essential for replenishing

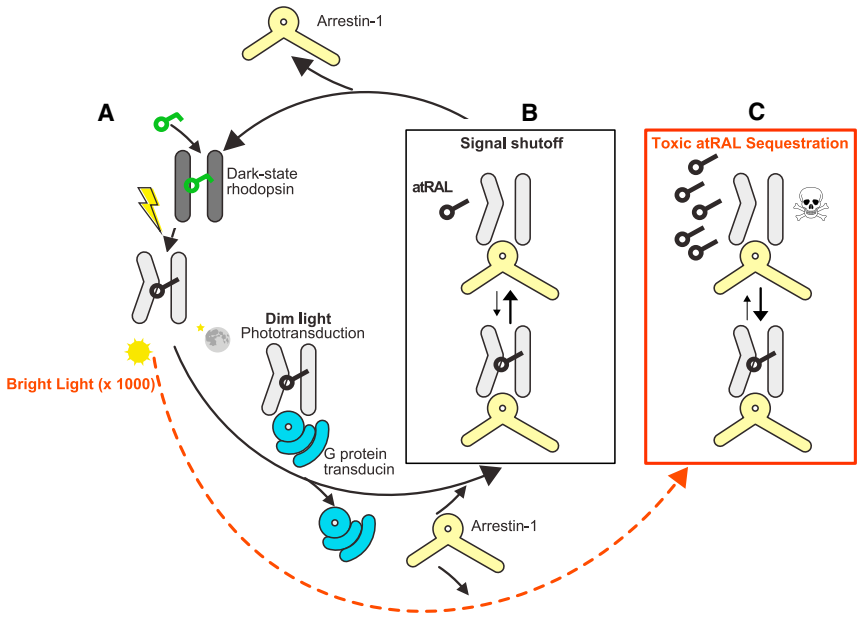

Figure 1. Arr-1 and RHO binding promotes sequestration of toxic all-*trans* retinal

(A) Schematic overview of RHO light activation mediated by 11-*cis*-retinal (green) photoisomerization to all-*trans* retinal (atRAL; black). In dim-light conditions, light-activated RHO (MII) is free to bind G protein transducin, initiating phototransduction.

(B) Signaling is quenched by Arr-1 binding, blocking transducin activation.

(C) Under bright light conditions, atRAL can be elevated to pathogenic levels, and Arr-1 is constitutively bound to RHO, promoting sequestration of toxic atRAL. Note that stoichiometry is simplified here, as are equilibria. For full details see main text and Sommer et al.,[2] Schafer et al.,[9] and Gurevich et al.[11]

the 11-*cis*-retinal chromophore required to regenerate RHO after light bleaches.[5] Arrestin-1 FL (Arr-1-FL) binding delays RHO regeneration with 11-*cis* retinal and increases the stability of the light-activated RHO (MII [metarhodopsin II]) conformation.[10] This stabilization delays the release of the toxic photoisomerized chromophore (all-*trans* retinal [atRAL]) from the MII binding pocket, promoting instead the re-uptake and re-binding of toxic all-*trans* retinal via MII conformational selectivity.[9,10] Arr-1 binding therefore promotes RHO-mediated sequestration of all-*trans* retinal, which may be photoprotective.[2,24] This putative function would be especially important in rods, where, unlike cones (which have an expanded retinoid recycling capacity[25,26]), all-*trans*-retinal clearance is limited by the activity of rod retinal dehydrogenases (RDH).[6,27,28] Exposure to bright light leads to all-*trans*-retinal release that can outpace clearance by visual cycle enzymes and transporters,[1,2] thus leading to accumulation of all-*trans* retinal and subsequent light-induced retinopathy through various modes of cellular toxicity involving oxidative stress and mitochondria-associated cell death.[6–8] All-*trans*-retinal-induced cell death is also associated with human eye diseases such as age-related macular degeneration, Stargardt disease, and others.[4,29,30]

In natural systems, photodamage risk via all-*trans*-retinal accumulation is predicted by both animal dim-light sensitivity as well as variation in ambient light conditions.[1,2] For instance, the rod-dominated retinas of some nocturnal rodents are more susceptible to photodamage than primates,[1,3] where photodamage risk is exacerbated by sudden changes in light intensity (e.g., bright light flashes) that lead to the rapid accumulation of all-*trans* retinal.[1,2,4] Based on these observations, we predicted that if Arr-1 does indeed play a role in photoprotection via RHO binding as previously proposed,[2] then we may expect to find functional adaptations within Arr-1 that enhance all-*trans*-retinal sequestration by RHO. We hypothesized that this may occur in animals at high risk of all-*trans*-retinal-mediated photodamage due to high rod densities and/or visual ecologies that introduce rapid changes in bright light exposure.

We hypothesized that these physiological and ecological risk factors would have altered Arr-1 functional constraints within particular animal lineages. We in turn predicted that this would be accompanied by shifts in selection pressure on *SAG* codons in dim-light-adapted animals vs. predominately diurnal outgroups. Using publicly available sequences and transcriptomes (Table S1), we constructed a large mammalian Arr-1 (*SAG*) phylogenetic dataset spanning most mammalian orders (Figure S1; Table S1). We validated all *SAG* sequences by constructing a gene tree using non-visual β-arrestins and cone arrestins as outgroups (Figures S1 and S2; Table S1; STAR Methods). We then used codon-based phylogenetic likelihood models[31] to perform a comprehensive characterization of selection pressures acting on *SAG* across different diurnal, nocturnal, and aquatic mammalian lineages (Figure 2A; Tables S2 and S3; STAR Methods). Briefly, mammalian Arr-1 sequences primarily evolved under purifying selection, with average d_N/d_S well below 1 (M0; M8a; Table S2). Subsequently, Clade model C (CmC) was used to explicitly compare d_N/d_S across different mammalian lineages. The best fitting model of these analyses identified significantly stronger selective constraint in non-echolocating bats and accelerated rates of evolution in cetaceans (Table S3). This was interesting because cetaceans are exposed to a wide variety of light intensities due to unique foraging behaviors such as deep diving and surfacing.[32–34] We next expanded the dataset to include avian and non-avian reptilian *SAG* (Tables S1 and S2), which allowed us to identify a parallel acceleration of *SAG* evolutionary rates in owls and cetaceans (Figure 2B; Table 1; STAR Methods). These are two dim-light specialist lineages with high rod densities that are at times exposed to bright light.[35–39] Interestingly, in both owl and cetacean *SAG*, we detected a parallel acceleration of evolutionary rates (Figure 2B) occurring within the Arr-1-FL domain responsible for binding RHO and promoting all-*trans*-retinal binding[10] (Figure 2C). This statistical signature was detected at Arr-1 sites 69 and 78 (Figures 2D and 2E) with high posterior probabilities (0.999 and 0.978, respectively). Cetaceans possess a rare amino acid variant at site 78 (K78) relative to other mammals (T/S78; Figure 2E), and this rare variant

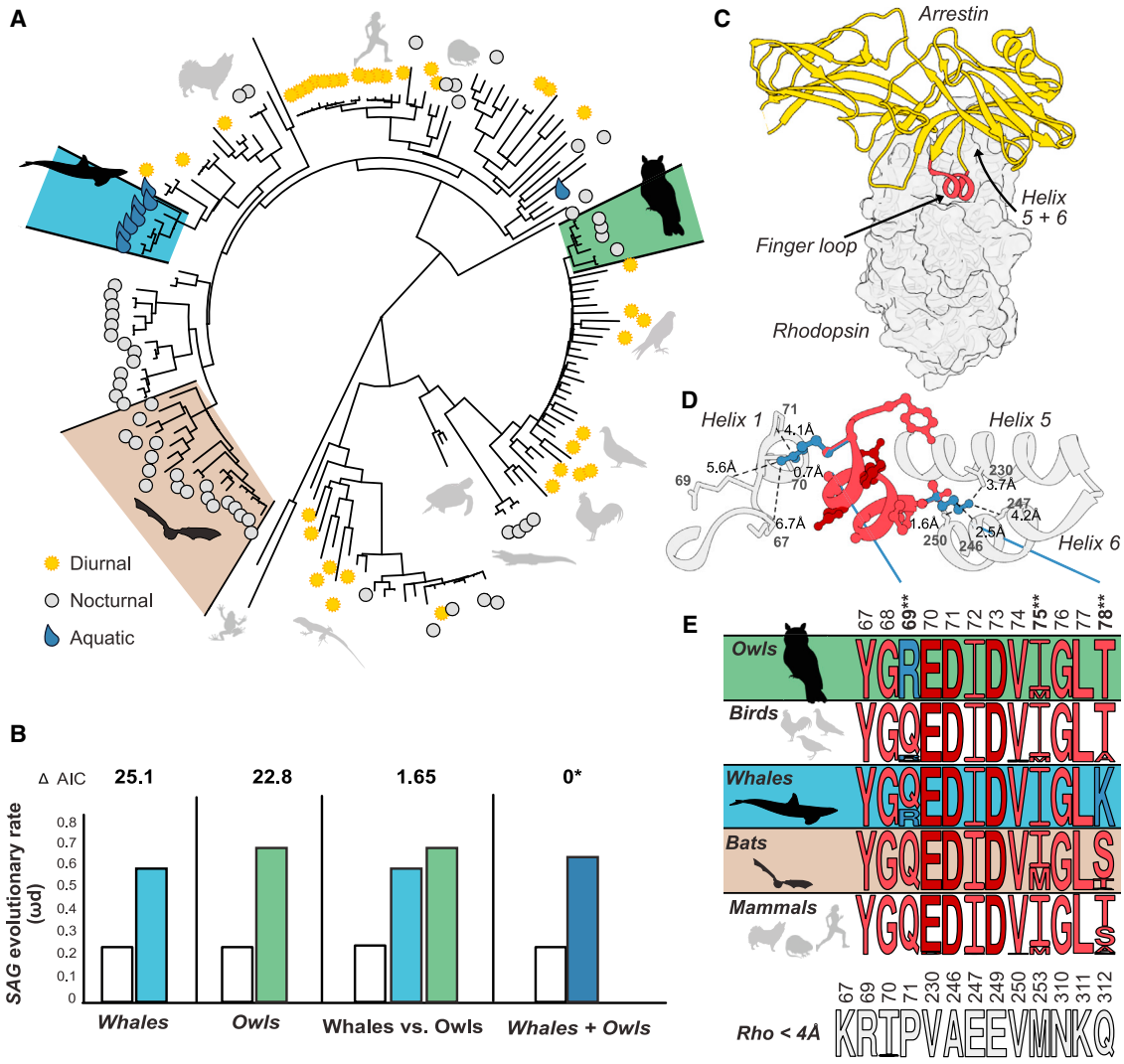

Figure 2. Convergent evolution of rare mutations in the rhodopsin (RHO) binding interface of owl and whale rod arrestin (Arr-1)

(A) Phylogeny used in statistical analyses of *SAG* evolutionary rates. Owl, whale (cetacean), and bat clades are highlighted. Diurnal, nocturnal, and aquatic visual ecologies are denoted.

(B) Statistical evidence for parallel molecular evolutionary rates (ω_d) between the *SAG* of owl (green) and whale (blue) clades, which are together divergent from that of other vertebrates (Table 1 [41]). Model fits were assessed by Akaike information criterion (ΔAIC) differences to the best fitting model.

(C) Crystal structure overview of the Arr-1-RHO complex (PDB: 4ZWJ). The FL domain of Arr-1 mediates binding to RHO.

(D and E) Zoom in of the Arr-1-FL (red) bound to RHO (grey). Arr-1 sites 69 and 78 are shown in blue (E). Arr-1 residues in this domain are highly conserved, except for rare variation in owls and whales at sites 69 and 78 (blue). These sites are under a parallel acceleration of evolutionary rates in whales and owls (**, Bayes empirical Bayes analysis >0.95[42]). RHO sites within 4Å of these Arr-1 positions are also highly conserved (grey). Note that the two mutations did not evolve simultaneously in the cetacean lineage.

See also Figures S1, S2, and S4; Tables S2 and S3; and STAR Methods.

appears to be fixed in cetacean Arr-1. We observed a second rare amino acid in the Arr1-FL (R69; Figure 2C) found only within whales that are deep-diving specialists[37,39] (Minke whale, *Balaenoptera acutorostrata*, and sperm whale, *Physeter catodon*). Strikingly, we also observed the Q69R substitution in the Arr-1 of all owl species we investigated here. Although the effects on all-*trans*-retinal sequestration are unknown, Q69R has been demonstrated to increase the binding strength of Arr-1 to RHO,[40] suggesting functional adaptation in whale and owl Arr-1. Importantly, our analysis demonstrates that RHO sites within the Arr-1 binding interface are tightly conserved across all species investigated here, indicating that the rare Arr-1 mutations in owl and whale species are unlikely to be second-order mutations accommodating hypothetical first-order mutations within owl and whale RHO (Figure 2E). Taken together, these findings suggest that natural selection may be driving convergent functional adaptation in the Arr-1 of owls and deep-diving whales.

The functional effects of these owl and whale Arr-1 variants (R69 and K78) on all-*trans*-retinal sequestration is unknown.

Table 1. Statistical evidence for convergent selection pressures acting on owl and whale rod arrestin (*SAG*)

Model & Foreground[a]	*ΔAIC*[b]	*ln*L	Parameters[c] ω_0	ω_1	ω_2/ω_d	Null	*p* [df][d]
M2a_rel	45.69	−31660.59	0.03 (58%)	1(7%)	0.24 (35%)	N/A	N/A
CmC_*Owls*	23.55	−31648.52	0.03 (57%)	1 (7%)	0.23 (36%) Owls: 0.73	M2a_rel	0.000 [1]
CmC_*Whales*	23.75	−31648.61	0.03 (59%)	1 (6%)	0.24 (34%) Whales: 0.64	M2a_rel	0.000 [1]
CmC_*OwlsWhales Convergent*	0*	−31636.74	0.03 (59%)	1 (6%)	0.24 (36%) OwlsWhales: 0.66	M2a_rel	0.000 [1]
CmC_*Owls* vs. *Whales (Divergent rates)*	1.66	−31636.57	0.03 (58%)	1 (6%)	0.23 (36%) Owls: 0.73 Whales: 0.61	M2a_rel CmC_Owl Whale Convergent	0.000 [2] 0.56 [1]

Abbreviations are as follows: *ln*L, ln Likelihood; *p*, p value; AIC, Akaike information criterion.
Results of Clade Model C (CmC) analyses of tetrapod *SAG* under various partitions.
[a]The foreground partition is listed after the underscore for the clade models and consists of either the clade of "owls" or the clade of "whales" . In any partitioning scheme, the entire clade was tested, and all non-foreground data are present in the background partition.
[b]All ΔAIC values are calculated from the lowest AIC model. The top best fit is marked with an asterisk (*).
[c]ω_d is the divergent site class, which has a separate value for the foreground and background partitions.
[d]Significant p values are $\alpha \leq 0.05$. Degrees of freedom are given in square brackets after the p values.

Thus, we used absorbance and fluorescence spectroscopy to experimentally investigate this. We utilized the model vertebrate RHO (bovine [*Bos taurus*]),[10,43] which we expressed and reconstituted *in vitro* within detergent micelles and made use of peptides representing the bovine Arr-1-FL and the bovine C-terminus of the G-transducin alpha subunit (Gtα CT). These peptides were nearly identical to those previously found to bind the RHO crevice and stabilize MII in a manner consistent with full-length Arr-1 and GtαCT[44,45] (STAR Methods). We extensively validated the function of these peptides in stabilizing MII, consistently reproducing the results of earlier studies (Figure S3; STAR Methods).[9,44–47] Briefly, the Arr-1-FL peptide stabilizes the RHO MII active state, promoting all-*trans*-retinal sequestration, and this is detected as the "incomplete decay" of MII by fluorescence spectroscopy (Figure 3A; [9]). We therefore employed this assay to test whether rare variants unique to owl and whale Arr-1 could potentially modulate and enhance all-*trans*-retinal sequestration by RHO MII. While the Arr-1-FL S78K substitution had no effect on incomplete MII decay, incredibly, we found that the Arr-1-FL Q69R substitution that convergently evolved in owls and whales significantly increased the rebinding of all-*trans* retinal by MII by nearly 30% (Figures 3B–3D). Structural modeling of Q69R reveals changes in proximity to nearby RHO residues (Figure S4), which suggest altered binding interactions between RHO and Arr-1 (STAR Methods). Although it was previously identified that Q69R increases the binding strength of full-length Arr-1 to the RHO active-state conformation,[40] it was previously unknown if these and other Arr-1 mutations could modulate and even enhance RHO-mediated sequestration of toxic all-*trans* retinal. Together with the evolutionary pressures selecting for this mutation, these results challenge our understanding of the physiological importance of Arr-1-RHO-mediated all-*trans*-retinal sequestration, suggesting the role of Arr-1 and RHO extend beyond canonical phototransduction and may have a role in photoprotection as previously suggested.[2,24]

The absence of this Arr-1 mutation from all other tetrapod Arr-1 to our knowledge, together with the complete conservation of RHO sites within the Arr1 binding interface (Figure 2E), strongly suggests that the presence of the rare Arr-1 R69 amino acid variant in owls and certain deep-diving cetaceans has evolved as a functional adaptation unique to these lineages. These lineages contain high rod densities and RHO expression—retinal features highly specialized to dim-light conditions that likely improve visual performance in their respective environments.[35,36] Thus, we might be tempted to speculate that stronger Arr-1-RHO binding resulting from the Arr-1 Q69R mutation may further enhance dim-light sensitivity, potentially by improving the functional roles of Arr-1 in RHO deactivation and dark adaptation.[49,50] However, the Q69R mutation increases binding promiscuity to other GPCRs,[40] which may interfere with the trafficking of non-visual GPCRs in the synaptic terminals of the rod photoreceptor.[11] This may be expected to interfere with rod signaling in the retina, which runs counter to the interpretation that enhanced Arr-1 binding to RHO is a dim-light adaptation. This is consistent with the extreme rarity of the Arr-1 Q69R mutation in tetrapods and suggests that this mutation may only be evolutionarily favorable if it presents a large physiological benefit.

We therefore propose an alternative interpretation in which the evolutionary selection patterns we detected were generated by the shared predisposition of owls and whales to photodamage; these lineages display high RHO expression and rod densities[35,36] and are unique among dim-light adapted lineages in their frequent exposure to vastly different light intensities due to intermittent diurnal activity in owls and surfacing behaviors in whales.[33,37–39] This combination of physiological and environmental variables is well-established to result in high photodamage risk.[1,2,4] Our interpretation is consistent with the "not just signal shutoff" function of Arr-1,[2] where the protein actively promotes RHO-mediated all-*trans*-retinal sequestration by forming heterotrimeric Arr-1-RHO complexes that are responsive to fluctuations in free all-*trans*-retinal levels that naturally occur within the retina *in vivo*.[4,10]

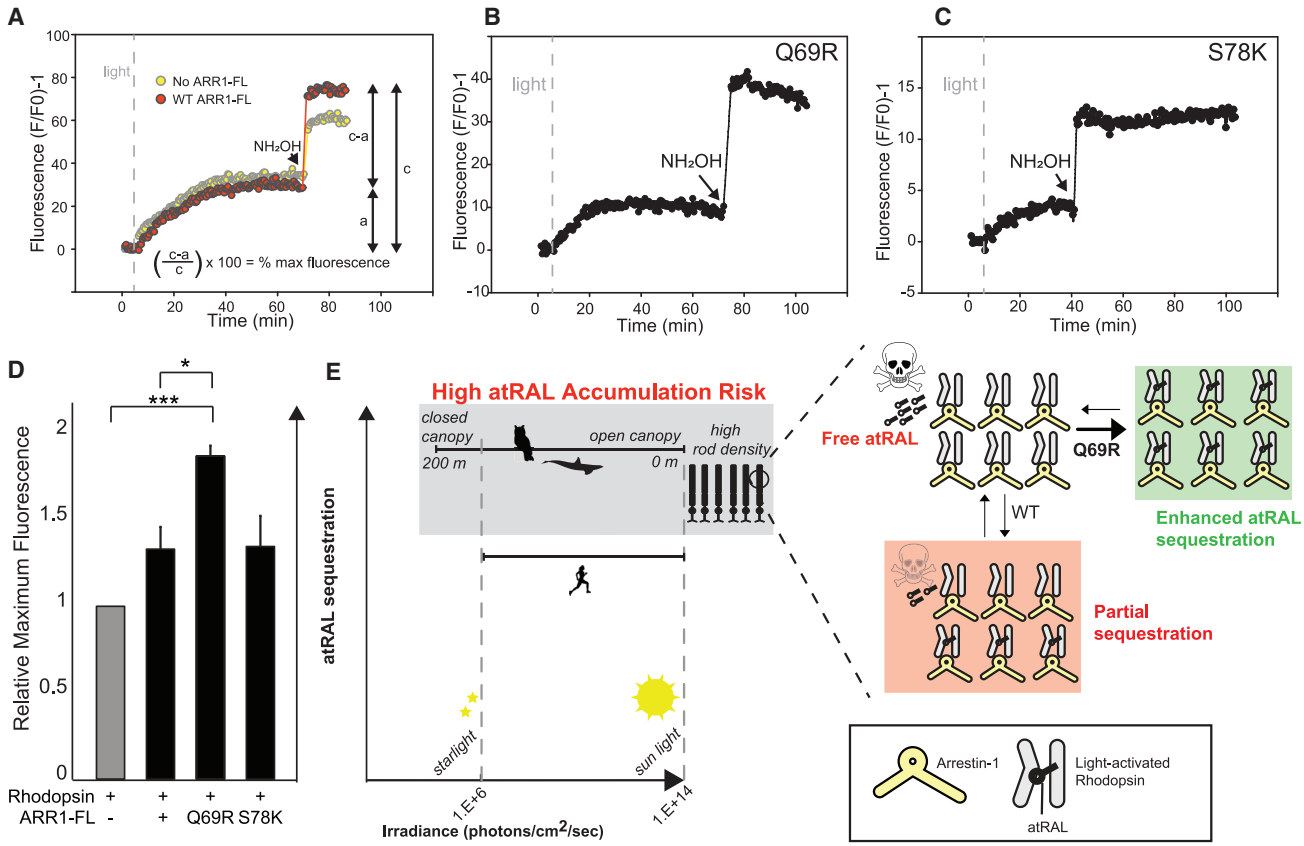

Figure 3. Owl and whale Arr-1 mutation (Q69R) enhances sequestration of toxic all-*trans* retinal (atRAL) by RHO

(A–C) Sequestration of toxic atRAL by RHO is detected as the incomplete decay of light-activated RHO (MII) using fluorescence spectroscopy, where complete release of atRAL is expedited by hydroxylamine (NH_2OH) addition.[9] atRAL sequestration is enhanced by the binding of wild-type (WT) and mutant (Q69R, S78K) Arr-1-FL peptides, which stabilize MII (STAR Methods).[9,10]

(D) Quantification of incomplete MII decay (calculation shown in [A]) with WT and mutant Arr-1-FL peptides is proportional to atRAL (atRAL) sequestration.[9] Significant differences were calculated using a two-sided t test. Standard error is shown.

(E) Light intensity ranges (solar irradiance) of owl, whale, and human natural environments[48] relative to expected atRAL sequestration by RHO-Arr-1 complexes shown in (D). High rod densities and RHO expression in owls and whales combines with changes in light exposure to produce high risk of atRAL accumulation (*see main text*). By increasing atRAL sequestration by ~30%, the Q69R mutation may mitigate atRAL toxicity in rod photoreceptors of owls and whales.

See also Figures S3 and S4, and Data S1A–S1C.

This putative role of Arr-1 requires further experimental investigation, especially since *in vivo* characterizations of Arr-1 -/- mice have detected neither any difference in all-*trans*-retinal reduction to all-*trans* retinol nor any difference in the rate of 11-*cis*-retinal regeneration levels; yet this likely reflects the complex temporal dynamics of retinoid metabolism, which are strongly determined by light intensity and duration and Arr-1 translocation time.[1,2] The challenge of recapitulating this complexity in the lab makes natural variation an especially valuable tool in elucidating how Arr-1 function may adapt to environmental light intensities over evolutionary timescales. The absence of the Q69R mutation from most tetrapods could also be related to the cytotoxicity of stable Arr1-RHO complexes in mammalian photoreceptors.[51] This may be related to the cell death promoted by some RHO mutations via AP-2 recruited clathrin vesicles signaled by Arr-1,[52] where Arr-1 with stronger binding and weaker oligomerization can lead to photoreceptor death.[53] Interestingly, Arr-1 self-association differs between species,[11] and in mice, there are also different pools of Arr-1 with different subcellular localizations.[54] This suggests myriad processes may be shifting in whales and owls to accommodate the evolution of enhanced Arr-1-FL binding to RHO. Variation in Arr1-related cytotoxicity may also explain why, in certain species, such as bats, all-*trans*-retinal sequestration may have been promoted instead by high intrinsic MII stability rather than through increases in Arr-1 Q69R binding strength.[24,33,55] Although owl RHO remains uncharacterized, RHO mutations have evolved in cetaceans that modulate MII stability through structural domains distal to the Arr-1 binding interface, occurring proximal to the retinal binding pocket (e.g., D83N, H195T, A292S, and A299S).[33,56,57] Indirect effects on RHO-Arr-1 interactions are possible, yet it is known that the openness of the chromophore binding pocket is an important determinant of MII decay and rod signaling.[58–60] Thus, the existence of RHO-intrinsic structural mechanisms for modulating MII stability raise the question as to why Arr-1 Q69R evolved if RHO-mediated all-*trans*-retinal sequestration can be shifted by RHO mutations alone.

A potential clue for the selective advantage of Arr-1 Q69R comes from studies of cetacean evolution, where the trade-off

between photoprotection (higher all-*trans*-retinal sequestration via high MII stability) and dark adaptation (rapid regeneration of dark-state RHO via low MII stability) appears particularly stark when comparing cetacean species. Specifically, low MII stability likely evolved during the terrestrial-to-aquatic transition in the whale ancestor, with selection favoring faster dark adaptation afforded by lower MII stability to match newly evolved deep-diving behavior.[33] Divergent evolutionary trajectories appear to have occurred since then, where MII stability increased in the orca but further decreased in the sperm whale[33,56,57]—one of the deep-diving specialists where we observed the Arr-1 Q69R mutation. Thus, these previous studies suggested that selection had "prioritized" more rapid RHO regeneration in the sperm whale as a deep-diving specialization.[39,56] *In vivo*, however, RHO does not function in isolation, where Arr-1 binding to RHO dimers is well-established to govern all-*trans*-retinal sequestration *or* release depending on high vs. low all-*trans*-retinal concentrations, respectively.[9,10,47] This balancing act appears to be further elaborated in the case in the sperm whale, potentially enabling it to benefit from the best of both worlds: under dim-light once RHO is released by Arr-1 (Figure 1B), an unstable MII enables dark-state RHO to rapidly regenerate[11,56]; under bright light, when RHO is bound by Arr-1 and MII is stabilized (Figure 1C),[10,40] Q69R would further enhance RHO-Arr-1 binding strength and therefore all-*trans*-retinal sequestration (Figure 3E). Our work therefore suggests that the photoprotection vs. dark adaption trade-off may at times be a false dichotomy—by targeting Arr-1 *and* RHO, selection may simultaneously weaken MII stability via RHO mutations (e.g., H195T) while also enhancing all-*trans*-retinal sequestration via Arr-1 mutations (e.g., Q69R). Through a co-evolutionary paradigm that operates on both RHO and Arr-1, these dynamics may explain how owls and deep-diving whales maintain the visual flexibility required to contend with the extremely variable light conditions of their unique habitats and behaviors.

Although only *in vivo* investigations can ultimately answer these questions, our work strongly suggests that natural selection has exploited the electrostatic interactions between Arr-1 and RHO to promote all-*trans*-retinal sequestration. This is of potentially vast clinical significance in human eye diseases associated with all-*trans*-retinal-induced cell death, such as age-related macular degeneration, Stargardt disease, and others.[4,29,30]

STAR★METHODS

Detailed methods are provided in the online version of this paper and include the following:

SUPPLEMENTAL INFORMATION

Supplemental information can be found online at https://doi.org/10.1016/j.cub.2023.09.015.

ACKNOWLEDGMENTS

The authors thank Sophia Chimenti, Alexandra Kraft, and Alexandra Rui Yue for their assistance with formatting the data. The authors acknowledge funding from the NSERC DG to B.S.W.C, and the UTSC and NSERC Postdoctoral Fellowships to F.E.H.

AUTHOR CONTRIBUTIONS

Conceptualization, G.M.C., R.K.S., B.S.W.C.; methodology, G.M.C., M.P., Y.L.I.C., N.B., R.K.S., B.S.W.C.; investigation, G.M.C., Y.L.I.C., E.d.A.G., A.V.N, F.E.H., N.B., R.K.S., B.S.W.C.; visualization, G.M.C., Y.L.I.C., A.V.N.; funding acquisition, B.S.W.C.; project administration, G.M.C., B.S.W.C.; supervision, G.M.C., N.B., B.S.W.C.; writing – original draft, G.M.C., Y.L.I.C., E.d.A.G., writing – review & editing, G.M.C., Y.L.I.C., E.d.A.G. , A.V.N., F.E.H., R.K.S., B.S.W.C.

DECLARATION OF INTERESTS

The authors declare no competing interests.

Received: June 17, 2023
Revised: August 21, 2023
Accepted: September 5, 2023
Published: September 29, 2023

REFERENCES

1. Rotanowska, M., and Sarna, T. (2005). Light-induced Damage to the Retina: Role of Rhodopsin Chromophore Revisited. Photochem. Photobiol. *81*, 1305–1330. https://doi.org/10.1562/2004-11-13-1R3-371.
2. Sommer, M.E., Hofmann, K.P., and Heck, M. (2014). Not just signal shutoff: the protective role of arrestin-1 in rod cells. Handb. Exp. Pharmacol. *219*, 101–116. https://doi.org/10.1007/978-3-642-41199-1_5.
3. Wenzel, A., Grimm, C., Samardzija, M., and Remé, C.E. (2005). Molecular mechanisms of light-induced photoreceptor apoptosis and neuroprotection for retinal degeneration. Prog. Retin. Eye Res. *24*, 275–306. https://doi.org/10.1016/j.preteyeres.2004.08.002.
4. Maeda, T., Golczak, M., and Maeda, A. (2012). Retinal photodamage mediated by all-trans-retinal. Photochem. Photobiol. *88*, 1309–1319. https://doi.org/10.1111/j.1751-1097.2012.01143.x.
5. Grimm, C., Wenzel, A., Hafezi, F., Yu, S., Redmond, T.M., and Remé, C.E. (2000). Protection of Rpe65-deficient mice identifies rhodopsin as a mediator of light-induced retinal degeneration. Nat. Genet. *25*, 63–66. https://doi.org/10.1038/75614.
6. Chen, Y., Okano, K., Maeda, T., Chauhan, V., Golczak, M., Maeda, A., and Palczewski, K. (2012). Mechanism of all-trans-retinal toxicity with implications for stargardt disease and age-related macular degeneration. J. Biol. Chem. *287*, 5059–5069. https://doi.org/10.1074/jbc.M111.315432.
7. Lee, K.A., Nawrot, M., Garwin, G.G., Saari, J.C., and Hurley, J.B. (2010). Relationships among visual cycle retinoids, rhodopsin phosphorylation, and phototransduction in mouse eyes during light and dark adaptation. Biochemistry *49*, 2454–2463. https://doi.org/10.1021/bi1001085.
8. Maeda, A., Maeda, T., Golczak, M., Chou, S., Desai, A., Hoppel, C.L., Matsuyama, S., and Palczewski, K. (2009). Involvement of all-trans-retinal

in acute light-induced retinopathy of mice. J. Biol. Chem. *284*, 15173–15183. https://doi.org/10.1074/jbc.M900322200.

9. Schafer, C.T., Fay, J.F., Janz, J.M., and Farrens, D.L. (2016). Decay of an active GPCR: Conformational dynamics govern agonist rebinding and persistence of an active, yet empty, receptor state. Proc. Natl. Acad. Sci. USA. *113*, 11961–11966. https://doi.org/10.1073/pnas.1606347113.
10. Sommer, M.E., Hofmann, K.P., and Heck, M. (2012). Distinct loops in arrestin differentially regulate ligand binding within the GPCR opsin. Nat. Commun. *3*, 995. https://doi.org/10.1038/ncomms2000.
11. Gurevich, V.V., Hanson, S.M., Song, X., Vishnivetskiy, S.A., and Gurevich, E.V. (2011). The functional cycle of visual arrestins in photoreceptor cells. Prog. Retin. Eye Res. *30*, 405–430. https://doi.org/10.1016/j.preteyeres.2011.07.002.
12. Gurevich, V.V., and Gurevich, E.V. (2014). Extensive shape shifting underlies functional versatility of arrestins. Curr. Opin. Cell Biol. *27*, 1–9. https://doi.org/10.1016/j.ceb.2013.10.007.
13. Hilger, D., Masureel, M., and Kobilka, B.K. (2018). Structure and dynamics of GPCR signaling complexes. Nat. Struct. Mol. Biol. *25*, 4–12. https://doi.org/10.1038/s41594-017-0011-7.
14. Smith, J.S., Lefkowitz, R.J., and Rajagopal, S. (2018). Biased signalling: from simple switches to allosteric microprocessors. Nat. Rev. Drug Discov. *17*, 243–260. https://doi.org/10.1038/nrd.2017.229.
15. Kang, Y., Zhou, X.E., Gao, X., He, Y., Liu, W., Ishchenko, A., Barty, A., White, T.A., Yefanov, O., Han, G.W., et al. (2015). Crystal structure of rhodopsin bound to arrestin by femtosecond X-ray laser. Nature *523*, 561–567. https://doi.org/10.1038/nature14656.
16. Latorraca, N.R., Wang, J.K., Bauer, B., Townshend, R.J.L., Hollingsworth, S.A., Olivieri, J.E., Xu, H.E., Sommer, M.E., and Dror, R.O. (2018). Molecular mechanism of GPCR-mediated arrestin activation. Nature *557*, 452–456. https://doi.org/10.1038/s41586-018-0077-3.
17. Sente, A., Peer, R., Srivastava, A., Baidya, M., Lesk, A.M., Balaji, S., Shukla, A.K., Babu, M.M., and Flock, T. (2018). Molecular mechanism of modulating arrestin conformation by GPCR phosphorylation. Nat. Struct. Mol. Biol. *25*, 538–545. https://doi.org/10.1038/s41594-018-0071-3.
18. Zhou, X.E., He, Y., de Waal, P.W., Gao, X., Kang, Y., Van Eps, N., Yin, Y., Pal, K., Goswami, D., White, T.A., et al. (2017). Identification of Phosphorylation Codes for Arrestin Recruitment by G Protein-Coupled Receptors. Cell *170*, 457–469.e13. https://doi.org/10.1016/j.cell.2017.07.002.
19. Indrischek, H., Prohaska, S.J., Gurevich, V.V., Gurevich, E.V., and Stadler, P.F. (2017). Uncovering missing pieces: duplication and deletion history of arrestins in deuterostomes. BMC Evol. Biol. *17*, 163. https://doi.org/10.1186/s12862-017-1001-4.
20. Sutton, R.B., Vishnivetskiy, S.A., Robert, J., Hanson, S.M., Raman, D., Knox, B.E., Kono, M., Navarro, J., and Gurevich, V.V. (2005). Crystal structure of cone arrestin at 2.3A: evolution of receptor specificity. J. Mol. Biol. *354*, 1069–1080. https://doi.org/10.1016/j.jmb.2005.10.023.
21. Gimenez, L.E., Vishnivetskiy, S.A., Baameur, F., and Gurevich, V.V. (2012). Manipulation of very few receptor discriminator residues greatly enhances receptor specificity of non-visual arrestins. J. Biol. Chem. *287*, 29495–29505. https://doi.org/10.1074/jbc.M112.366674.
22. Ernst, O.P., Lodowski, D.T., Elstner, M., Hegemann, P., Brown, L.S., and Kandori, H. (2014). Microbial and animal rhodopsins: structures, functions, and molecular mechanisms. Chem. Rev. *114*, 126–163. https://doi.org/10.1021/cr4003769.
23. Hao, W., Wenzel, A., Obin, M.S., Chen, C.K., Brill, E., Krasnoperova, N.V., Eversole-Cire, P., Kleyner, Y., Taylor, A., Simon, M.I., et al. (2002). Evidence for two apoptotic pathways in light-induced retinal degeneration. Nat. Genet. *32*, 254–260. https://doi.org/10.1038/ng984.
24. Castiglione, G.M., and Chang, B.S. (2018). Functional trade-offs and environmental variation shaped ancient trajectories in the evolution of dim-light vision. Elife *7*, e35957, https://doi.org/10.7554/eLife.35957.
25. Tsybovsky, Y., and Palczewski, K. (2015). Retinoid Pathway Gene Mutations and the Pathophysiology of Related Visual Diseases. In The Retinoids, P. Dolle, and K. Neiderreither, eds. (John Wiley & Sons, Inc.), pp. 529–542. https://doi.org/10.1002/9781118628003.ch24.
26. Wang, J.S., and Kefalov, V.J. (2011). The cone-specific visual cycle. Prog. Retin. Eye Res. *30*, 115–128. https://doi.org/10.1016/j.preteyeres.2010.11.001.
27. Chen, C., Thompson, D.A., and Koutalos, Y. (2012). Reduction of all-trans-retinal in vertebrate rod photoreceptors requires the combined action of RDH8 and RDH12. J. Biol. Chem. *287*, 24662–24670. https://doi.org/10.1074/jbc.M112.354514.
28. Saari, J.C., Garwin, G.G., Van Hooser, J.P., and Palczewski, K. (1998). Reduction of all-trans-retinal limits regeneration of visual pigment in mice. Vision Res. *38*, 1325–1333. https://doi.org/10.1016/S0042-6989(97)00198-3.
29. Molday, R.S., Zhong, M., and Quazi, F. (2009). The role of the photoreceptor ABC transporter ABCA4 in lipid transport and Stargardt macular degeneration. Biochim. Biophys. Acta *1791*, 573–583. https://doi.org/10.1016/j.bbalip.2009.02.004.
30. Sparrow, J.R., Wu, Y., Kim, C.Y., and Zhou, J. (2010). Phospholipid meets all-trans-retinal: the making of RPE bisretinoids. J. Lipid Res. *51*, 247–261. https://doi.org/10.1194/jlr.R000687.
31. Yang, Z. (2007). PAML 4: phylogenetic analysis by maximum likelihood. Mol. Biol. Evol. *24*, 1586–1591. https://doi.org/10.1093/molbev/msm088.
32. Denton, E.J. (1990). Light and vision at depths greater than 200 metres. In Light and Life in the Sea, P.J. Herring, A.K. Campbell, M. Whitfield, and L. Maddock, eds. (Cambridge University Press), pp. 127–148.
33. Dungan, S.Z., and Chang, B.S.W. (2022). Ancient whale rhodopsin reconstructs dim-light vision over a major evolutionary transition: Implications for ancestral diving behavior. Proc. Natl. Acad. Sci. USA. *119*, e2118145119, https://doi.org/10.1073/pnas.2118145119.
34. Warrant, E.J., and Johnsen, S. (2013). Vision and the light environment. Curr. Biol. *23*, R990–R994. https://doi.org/10.1016/j.cub.2013.10.019.
35. Höglund, J., Mitkus, M., Olsson, P., Lind, O., Drews, A., Bloch, N.I., Kelber, A., and Strandh, M. (2019). Owls lack UV-sensitive cone opsin and red oil droplets, but see UV light at night: Retinal transcriptomes and ocular media transmittance. Vision Res. *158*, 109–119. https://doi.org/10.1016/j.visres.2019.02.005.
36. Peichl, L., Behrmann, G., and Kröger, R.H. (2001). For whales and seals the ocean is not blue: a visual pigment loss in marine mammals. Eur. J. Neurosci. *13*, 1520–1528. https://doi.org/10.1046/j.0953-816x.2001.01533.x.
37. Blix, A.S., and Folkow, L.P. (1995). Daily energy expenditure in free living minke whales. Acta Physiol. Scand. *153*, 61–66. https://doi.org/10.1111/j.1748-1716.1995.tb09834.x.
38. Li, Z., Stidham, T.A., Zheng, X., Wang, Y., Zhao, T., Deng, T., and Zhou, Z. (2022). Early evolution of diurnal habits in owls (Aves, Strigiformes) documented by a new and exquisitely preserved Miocene owl fossil from China. Proc. Natl. Acad. Sci. USA. *119*, e2119217119, https://doi.org/10.1073/pnas.2119217119.
39. Watkins, W.A., Daher, M.A., Fristrup, K.M., Howald, T.J., and Di Sciara, G.N. (1993). SPERM WHALES TAGGED WITH TRANSPONDERS AND TRACKED UNDERWATER BY SONAR. Mar. Mamm. Sci. *9*, 55–67. https://doi.org/10.1111/j.1748-7692.1993.tb00426.x.
40. Vishnivetskiy, S.A., Gimenez, L.E., Francis, D.J., Hanson, S.M., Hubbell, W.L., Klug, C.S., and Gurevich, V.V. (2011). Few residues within an extensive binding interface drive receptor interaction and determine the specificity of arrestin proteins. J. Biol. Chem. *286*, 24288–24299. https://doi.org/10.1074/jbc.M110.213835.
41. Castiglione, G.M., Schott, R.K., Hauser, F.E., and Chang, B.S.W. (2018). Convergent selection pressures drive the evolution of rhodopsin kinetics at high altitudes via nonparallel mechanisms. Evolution *72*, 170–186. https://doi.org/10.1111/evo.13396.
42. Yang, Z., Wong, W.S.W., and Nielsen, R. (2005). Bayes empirical bayes inference of amino acid sites under positive selection. Mol. Biol. Evol. *22*, 1107–1118. https://doi.org/10.1093/molbev/msi097.

43. Choe, H.W., Kim, Y.J., Park, J.H., Morizumi, T., Pai, E.F., Krauss, N., Hofmann, K.P., Scheerer, P., and Ernst, O.P. (2011). Crystal structure of metarhodopsin II. Nature *471*, 651–655. https://doi.org/10.1038/nature09789.

44. Elgeti, M., Kazmin, R., Rose, A.S., Szczepek, M., Hildebrand, P.W., Bartl, F.J., Scheerer, P., and Hofmann, K.P. (2018). The arrestin-1 finger loop interacts with two distinct conformations of active rhodopsin. J. Biol. Chem. *293*, 4403–4410. https://doi.org/10.1074/jbc.M117.817890.

45. Szczepek, M., Beyrière, F., Hofmann, K.P., Elgeti, M., Kazmin, R., Rose, A., Bartl, F.J., von Stetten, D., Heck, M., Sommer, M.E., et al. (2014). Crystal structure of a common GPCR-binding interface for G protein and arrestin. Nat. Commun. *5*, 4801. https://doi.org/10.1038/ncomms5801.

46. Kisselev, O.G., Meyer, C.K., Heck, M., Ernst, O.P., and Hofmann, K.P. (1999). Signal transfer from rhodopsin to the G-protein: evidence for a two-site sequential fit mechanism. Proc. Natl. Acad. Sci. USA. *96*, 4898–4903. https://doi.org/10.1073/pnas.96.9.4898.

47. Sommer, M.E., Smith, W.C., and Farrens, D.L. (2006). Dynamics of Arrestin-Rhodopsin Interactions. J. Biol. Chem. *281*, 9407–9417. https://doi.org/10.1074/jbc.M510037200.

48. Cronin, T., Johnsen, S., Marshall, N.J., and Warrant, E.J. (2014). Visual Ecology (Princeton University Press).

49. Schröder, K., Pulvermüller, A., and Hofmann, K.P. (2002). Arrestin and its splice variant Arr1-370A (p44). Mechanism and biological role of their interaction with rhodopsin. J. Biol. Chem. *277*, 43987–43996. https://doi.org/10.1074/jbc.M206211200.

50. Frederiksen, R., Nymark, S., Kolesnikov, A.V., Berry, J.D., Adler, L., 4th, Koutalos, Y., Kefalov, V.J., and Cornwall, M.C. (2016). Rhodopsin kinase and arrestin binding control the decay of photoactivated rhodopsin and dark adaptation of mouse rods. J. Gen. Physiol. *148*, 1–11. https://doi.org/10.1085/jgp.201511538.

51. Chen, J., Shi, G., Concepcion, F.A., Xie, G., Oprian, D., and Chen, J. (2006). Stable rhodopsin/arrestin complex leads to retinal degeneration in a transgenic mouse model of autosomal dominant retinitis pigmentosa. J. Neurosci. *26*, 11929–11937. https://doi.org/10.1523/JNEUROSCI.3212-06.2006.

52. Moaven, H., Koike, Y., Jao, C.C., Gurevich, V.V., Langen, R., and Chen, J. (2013). Visual arrestin interaction with clathrin adaptor AP-2 regulates photoreceptor survival in the vertebrate retina. Proc. Natl. Acad. Sci. USA. *110*, 9463–9468. https://doi.org/10.1073/pnas.1301126110.

53. Song, X., Seo, J., Baameur, F., Vishnivetskiy, S.A., Chen, Q., Kook, S., Kim, M., Brooks, E.K., Altenbach, C., Hong, Y., et al. (2013). Rapid degeneration of rod photoreceptors expressing self-association-deficient arrestin-1 mutant. Cell. Signal. *25*, 2613–2624. https://doi.org/10.1016/j.cellsig.2013.08.022.

54. Cleghorn, W.M., Tsakem, E.L., Song, X., Vishnivetskiy, S.A., Seo, J., Chen, J., Gurevich, E.V., and Gurevich, V.V. (2011). Progressive reduction of its expression in rods reveals two pools of arrestin-1 in the outer segment with different roles in photoresponse recovery. PLoS One *6*, e22797, https://doi.org/10.1371/journal.pone.0022797.

55. Gutierrez, E.d.A., Castiglione, G.M., Morrow, J.M., Schott, R.K., Loureiro, L.O., Lim, B.K., and Chang, B.S.W. (2018). Functional Shifts in Bat Dim-Light Visual Pigment Are Associated with Differing Echolocation Abilities and Reveal Molecular Adaptation to Photic-Limited Environments. Mol. Biol. Evol. *35*, 2422–2434. https://doi.org/10.1093/molbev/msy140.

56. Gai, Y., Tian, R., Liu, F., Mu, Y., Shan, L., Irwin, D.M., Liu, Y., Xu, S., and Yang, G. (2023). Diversified Mammalian Visuasl Adaptations to Bright- or Dim-Light Environments. Mol. Biol. Evol. *40*, msad063, https://doi.org/10.1093/molbev/msad063.

57. Dungan, S.Z., and Chang, B.S.W. (2017). Epistatic interactions influence terrestrial–marine functional shifts in cetacean rhodopsin. Proc. Biol. Sci. *284*, 20162743, https://doi.org/10.1098/rspb.2016.2743.

58. Piechnick, R., Ritter, E., Hildebrand, P.W., Ernst, O.P., Scheerer, P., Hofmann, K.P., and Heck, M. (2012). Effect of channel mutations on the uptake and release of the retinal ligand in opsin. Proc. Natl. Acad. Sci. USA. *109*, 5247–5252. https://doi.org/10.1073/pnas.1117268109.

59. Yue, W.W.S., Frederiksen, R., Ren, X., Luo, D.G., Yamashita, T., Shichida, Y., Cornwall, M.C., and Yau, K.W. (2017). Spontaneous activation of visual pigments in relation to openness/closedness of chromophore-binding pocket. Elife *6*, e18492, https://doi.org/10.7554/eLife.18492.

60. Wald, G., Brown, P.K., and Kennedy, D. (1957). THE VISUAL SYSTEM OF THE ALLIGATOR. J. Gen. Physiol. *40*, 703–713. https://doi.org/10.1085/jgp.40.5.703.

61. Hedges, S.B., Marin, J., Suleski, M., Paymer, M., and Kumar, S. (2015). Tree of life reveals clock-like speciation and diversification. Mol. Biol. Evol. *32*, 835–845. https://doi.org/10.1093/molbev/msv037.

62. Löytynoja, A., and Goldman, N. (2010). webPRANK: a phylogeny-aware multiple sequence aligner with interactive alignment browser. BMC Bioinf. *11*, 579. https://doi.org/10.1186/1471-2105-11-579.

63. Guindon, S., Dufayard, J.F., Lefort, V., Anisimova, M., Hordijk, W., and Gascuel, O. (2010). New algorithms and methods to estimate maximum-likelihood phylogenies: assessing the performance of PhyML 3.0. Syst. Biol. *59*, 307–321. https://doi.org/10.1093/sysbio/syq010.

64. Foley, N.M., Springer, M.S., and Teeling, E.C. (2016). Mammal madness: is the mammal tree of life not yet resolved? Philos. Trans. R. Soc. Lond. B Biol. Sci. *371*, 20150140, https://doi.org/10.1098/rstb.2015.0140.

65. Prum, R.O., Berv, J.S., Dornburg, A., Field, D.J., Townsend, J.P., Lemmon, E.M., and Lemmon, A.R. (2015). A comprehensive phylogeny of birds (Aves) using targeted next-generation DNA sequencing. Nature *526*, 569–573. https://doi.org/10.1038/nature15697.

66. Amemiya, C.T., Alföldi, J., Lee, A.P., Fan, S., Philippe, H., Maccallum, I., Braasch, I., Manousaki, T., Schneider, I., Rohner, N., et al. (2013). The African coelacanth genome provides insights into tetrapod evolution. Nature *496*, 311–316. https://doi.org/10.1038/nature12027.

67. Schott, R.K., Van Nynatten, A., Card, D.C., Castoe, T.A., and S W Chang, B. (2018). Shifts in Selective Pressures on Snake Phototransduction Genes Associated with Photoreceptor Transmutation and Dim-Light Ancestry. Mol. Biol. Evol. *35*, 1376–1389. https://doi.org/10.1093/molbev/msy025.

68. Bielawski, J.P., and Yang, Z. (2004). A maximum likelihood method for detecting functional divergence at individual codon sites, with application to gene family evolution. J. Mol. Evol. *59*, 121–132. https://doi.org/10.1007/s00239-004-2597-8.

69. Weadick, C.J., and Chang, B.S.W. (2012). An improved likelihood ratio test for detecting site-specific functional divergence among clades of protein-coding genes. Mol. Biol. Evol. *29*, 1297–1300. https://doi.org/10.1093/molbev/msr311.

70. Govardovskii, V.I., Fyhrquist, N., Reuter, T., Kuzmin, D.G., and Donner, K. (2000). In search of the visual pigment template. Vis. Neurosci. *17*, 509–528. https://doi.org/10.1017/s0952523800174036.

71. Schleicher, A., Kühn, H., and Hofmann, K.P. (1989). Kinetics, binding constant, and activation energy of the 48-kDa protein-rhodopsin complex by extra-metarhodopsin II. Biochemistry *28*, 1770–1775. https://doi.org/10.1021/bi00430a052.

72. Zhao, D.Y., Pöge, M., Morizumi, T., Gulati, S., Van Eps, N., Zhang, J., Miszta, P., Filipek, S., Mahamid, J., Plitzko, J.M., et al. (2019). Cryo-EM structure of the native rhodopsin dimer in nanodiscs. J. Biol. Chem. *294*, 14215–14230. https://doi.org/10.1074/jbc.RA119.010089.

73. Lally, C.C.M., Bauer, B., Selent, J., and Sommer, M.E. (2017). C-edge loops of arrestin function as a membrane anchor. Nat. Commun. *8*, 14258, https://doi.org/10.1038/ncomms14258.

74. Pettersen, E.F., Goddard, T.D., Huang, C.C., Couch, G.S., Greenblatt, D.M., Meng, E.C., and Ferrin, T.E. (2004). UCSF Chimera–a visualization system for exploratory research and analysis. J. Comput. Chem. *25*, 1605–1612. https://doi.org/10.1002/jcc.20084.

STAR★METHODS

KEY RESOURCES TABLE

REAGENT or RESOURCE	SOURCE	IDENTIFIER
Antibodies		
1D4 monoclonal antibody	https://doi.org/10.1007/978-1-4939-1034-2_1	RRID: AB_304874
Chemicals, peptides, and recombinant proteins		
11-cis retinal	Dr. Rosalie Crouch, Medical University of South Carolina	N/A
Arrestin-1 and of GtαCT-HA peptides	GL Biochem (Shanghai)	N/A
Critical commercial assays		
Lipofectamine 2000	ThermoFisher Scientific	Catalog Number: 11668019
Ultralink Hydrazide Resin	ThermoFisher Scientific	Catalog Number: 53149
Experimental models: Cell lines		
HEK293T (*Homo sapiens*)	Dr. David Hampson, University of Toronto	N/A
Recombinant DNA		
Bos taurus RHO	Integrated DNA Technologies	Accession: M12689
pIRES-hrGFP II	Stratagene	Addgene: Plasmid #71317
Software and algorithms		
PAML 4.7	https://doi.org/10.1093/molbev/msm088	N/A
MODELLER	https://doi.org/10.1002/cpbi.3	N/A

RESOURCE AVAILABILITY

Lead contact

Further information and requests for resources and reagents should be directed to and will be fulfilled by the lead contact, Gianni Castiglione (gianni.castiglione@vanderbilt.edu).

Materials availability

Plasmids generated in this study are available upon request. All sequences used in this study were obtained from NCBI and are described in manuscript tables.

Data and code availability

This paper analyzes existing, publicly available data. The accession numbers for the datasets are listed in the supplemental information. All *RH1/RHO* and *SAG* sequences analyzed in this study were obtained from NCBI with accessions described in manuscript tables. Experimental data generated in this study are available within the manuscript and supplemental information. Any additional information required to reanalyze the data reported in this paper is available from the lead contact upon request.

EXPERIMENTAL MODEL AND STUDY PARTICIPANT DETAILS

Cell lines

HEK293T (*Homo sapiens*) cells were used for heterologous expression of bovine rhodopsin (RHO). These cells were obtained from Dr. David Hampson (University of Toronto) and authenticated by STR profiling. Cells were cultured at 37°C, under 5% CO_2.

METHOD DETAILS

Dataset assembly

Arrestin-1 coding sequences (*SAG*) representing all major tetrapod phylogenetic groupings (Figure S1; Table S1)[61] were obtained from GenBank. Additional *SAG* coding-sequences were manually assembled from publicly available transcriptome sequences

(Table S1) of paired Illumina reads. Reads were trimmed using TrimmomaticPE v8.25, and Trinity (v2.4.0) was run with regular defaults. Redundant contigs were removed (cd-hit-est v4.6) and then BLASTed (blastn v2.2.31+) against a reference sequence (*Tyto alba SAG*; XM_009967181.1) to annotate relevant contigs through a custom pipeline. Relevant contigs were constructed using a custom Python script. A *SAG* alignment was then generated using PRANK codon alignment,[62] followed by manual adjustment. All sequences were confirmed as rod arrestin (*SAG*) by phylogenetic analysis with cone arrestin (*ARR3*) and non-visual beta arrestin (ARR2B) coding sequences (Figure S1). Briefly, a gene tree was constructed in PHYML 3.0, using Akaike information criterion (AIC) automatic model selection, a BIONJ starting tree with NNI tree improvement, and aLRT SH-like branch support[63](Figure S1). The final *SAG* alignment encoded for arrestin-1 amino acid residues 26-366 (human ARR1 numbering; Uniprot OX_9606). Using this alignment, we pruned clades into separate *SAG* datasets: (1) Tetrapods; (2) Mammals. For each dataset, a species tree was constructed (Figure S2) by reference to established relationships for Tetrapods.[61,64–67] Sequences not spanning residues 26-366 (human ARR1 numbering; Uniprot OX_9606) were pruned. This alignment and the species tree were used in molecular evolutionary analyses.

Molecular evolutionary analyses

We used codon models of molecular evolution from the PAML 4.7 software package[31] to characterize mammals, bats, and cetacean *SAG*. First, we estimated the evolutionary rates (d_N/d_S) within the mammalian dataset using the random sites models (M1, M2, M3, M7, M8) implemented in the CODEML program (Table S2). Next we employed PAML Clade model C (CmC)[68] to explicitly test for long-term shifts in evolutionary rates (d_N/d_S) between foreground and background branches or clades within the tetrapod and mammalian *SAG* datasets (Tables 1 and S3). In any partitioning scheme, all non-foreground data are present in the background partition. The foreground partition is listed after the underscore for the clade models (e.g., CmC_*foreground*). M2aREL was used as the null model to determine statistical significance via a likelihood-ratio test (LRT) against a X^2 distribution.[69] Parallel shifts in selective constraint in owl and whale *SAG* was tested for by conducting explicit tests of divergence in *SAG* evolutionary rates, as previously described.[41] Briefly, this was done by conducting a CmC analysis on an alternative partitioning scheme treating each clade separately, and comparing the likelihood fit of that alternative model against the nested null CmC model treating the owl and whale clades as a single partition, using a LRT (Table 1). CmC estimated site-specific posterior probabilities for respective molecular evolutionary tests. We consulted the posterior probabilities produced by the Bayes empirical Bayes (BEB) analysis[42] For all PAML models, multiple runs with different starting priors were carried out to check for the convergence of parameter estimates. Significant differences in model fits were determined by LRT. The best fitting model for each dataset was assessed by differences in AIC. Using codon-based phylogenetic likelihood models, we detected significant evidence of accelerated evolutionary rates in both cetacean ($p < 0.000$) and owl *SAG* ($p < 0.000$) relative to all other tetrapods (Figure 2B; Table 1). Due to this similarity, we next tested whether the accelerated evolutionary rates within the *SAG* of these dim-light specialists could be better described with a single evolutionary rate parameter (ω_d), which would be evidence for a convergent shift in both dim-light specialists relative to other tetrapods.[41] We found highly significant evidence for parallel shifts in evolutionary rates between cetacean and owl *SAG*, outperforming the previously tested models (Table 1). We then tested the alternative hypothesis that cetacean and owl groups displayed selection pressures distinct from each other by using an owl and whale two-partition model estimating a separate ω_d for cetaceans, owls, and other tetrapods (Figure 2B; Table 1). A likelihood-ratio test (LRT) with the one-partition owl and whale model as the nested null hypothesis rejected this alternative model ($p = 0.56$; Table 1), providing evidence for the sufficiency of a single evolutionary rate parameter to describe the similar shifts in the selective constraints acting on each dim-light *SAG* relative to other tetrapods.

RHO expression and spectroscopic assays with synthetic peptides

The complete coding sequence of bovine (*Bos taurus*) RHO in the pJET1.2 cloning vector (ThermoFisher Scientfic), as described in a previous study was used here.[24] All sequences were verified using a 3730 DNA Analyzer (Applied Biosystems) at the Centre for Analysis of Genome Evolution and Function (CAGEF) at the University of Toronto. Wild type and mutant RHO sequences were transferred to the pIRES-hrGFP II expression vector (Stratagene) for subsequent transient transfection of HEK293T cells (8 μg per 10 cm plate) using Lipofectamine 2000 (Invitrogen). HEK293T cells were obtained from David Hampson (University of Toronto), were authenticated by STR profiling (Centre for Applied Genomics, The Hospital for Sick Children) and tested negative for mycoplasma contamination. Media was changed after 24 h, and cells were harvested 48 h post-transfection. Cells were washed twice with harvesting buffer (PBS, 10 μg/mL aprotinin, 10 μg/mL leupeptin), and RHO protein were regenerated for 2 h in the dark with 5 μM 11-*cis*-retinal generously provided by Dr. Rosalie Crouch (Medical University of South Carolina). After regeneration, the samples were incubated at 4°C in solubilization buffer (50 mM Tris pH 6.8, 100 mM NaCl, 1 mM CaCl2, 1% dodecylmaltoside, 0.1 mM PMSF) for 2 h and immunoaffinity purified overnight using the 1D4 monoclonal antibody coupled to the UltraLink Hydrazide Resin (ThermoFisher Scientific). Resin was washed three times with wash buffer 1 (50 mM Tris pH 7.0, 100 mM NaCl, 0.1% dodecylmaltoside) and twice using wash buffer 2 (50 mM sodium phosphate, 0.1% dodecylmaltoside; pH 7.0). RHOs were eluted from the UltraLink resin using 5 mg/mL of a 1D4 peptide, consisting of the last 9 amino acids of bovine RHO (TETSQVAPA).

All peptides used are based on WT bovine background and were synthesized by GL Biochem (Shanghai) Ltd with >98% purity verified by high-performance liquid chromatography and mass spectrometry. The high affinity C-terminus transducin (Gt_aCT-HA) peptide[45] has a K341L substitution in comparison to the WT bovine transducin. Whereas the WT bovine Arr-1 FL (finger loop) peptide is identical to the one used in[45] but extends to site 79 instead of 77. Arr1-FL peptides containing single amino acid substitutions (Q69R and S78K) were also synthesized. The Arr-1 and GtαCT-HA peptides were nearly identical to those previously found to bind the RHO crevice and stabilize metarhodopsin II (MII) in a manner consistent with full-length Arr-1 and GtαCT.[44,45]

For absorbance spectroscopy assays, peptides were solubilized in wash buffer 2 and incubated with 0.6uM purified RHO for 10 min on ice. Initial incubation time was based on a previous study (5 min[45]) but after optimization in our system we found 10 min was ideal for each peptide. Binding of Arr-1 peptides to RHO is of low efficiency relative to that of Gt_aCT-HA peptides, which is likely due to the absence of other Arr-1 domains present in the full-length protein.[45] Arr-1 peptide concentration (3mM) was based on titration optimization conducted in this study and that done previously.[45] The UV-visible absorption spectra of purified rho samples with and without peptides (Figure S3) were recorded in the dark at 0°C using a Cary 4000 double-beam absorbance spectrophotometer (Agilent). All wavelength of maximum absorbance (λ_{MAX}) values were determined by fitting dark spectra to a standard template curve for A1 visual pigments.[70] RHO samples were light-activated for 30 s using a fiber optic lamp (Dolan-Jenner), resulting in a shift in λ_{MAX} to ~380 nm, characteristic of the biologically active MII intermediate.[71] We used the extra MII assay to validate whether GtαCT-HA and Arr1-FL peptides bound and stabilized the MII active-state of RHO over the MI species similar to full-length Gt and Arr1 as described previously.[45,46,71] Briefly, extra MII is defined as the additional MII formed in the presence of peptide. We measured the difference between absorbance values at MII (380 nm) and MI/MII isosbestic point (417 nm), a reference point that stays constant, in the dark and after light-bleach to calculate % change as an indicator of extra MII formation as represented in the equation (Bleached Abs_{380nm}-Abs_{417nm}) - (Dark Abs_{380nm}-Abs_{417nm}). Relative extra MII formation values were calculated by normalizing to the no-peptide control and indicates the additional MII formation in comparison to the no peptide control (Data S1A). In titrations of GtαCT-HA or Arr1-FL peptides (Figure S3), the data points were fitted to 1-site saturation equation $y = B_{max}*x/ (K_D + x)$, with B_{max} as the efficacy and K_D as the binding affinity extra-MII (i.e., %MII), as previously described.[10] The GtαCT-HA peptide binds MII with high affinity[44–46] and served as a positive control for our spectroscopic assays. Using the 'Extra-MII' absorbance spectroscopic assay,[71] we found that the Arr-1-FL peptide stabilized the 380 nm-absorbing MII species over the preceding MI species (Figure S3), indicating that Arr1-FL peptides are binding the active state (MII) of RHO within detergent micelles.[45,46,71] Titration analysis indicated KD values of 60.9 μM and ~3.19 mM for GtαCT-HA and Arr-1-FL peptides (Figure S3), respectively, consistent with previous studies.[44–46]

We investigated incomplete MII decay using fluorescence spectroscopy to measure retinal release in the presence of GtαCT-HA and Arr1-FL peptides, which reflects retinal re-uptake by RHO via peptide-mediated stabilization of MII.[9,10] Briefly, this assay detected increasing fluorescence as a result of decreased quenching of intrinsic tryptophan fluorescence at W265 by the retinal chromophore, and is a reliable proxy of the conformational decay of MII.[9] Retinal release following RHO photoactivation was monitored using a Cary Eclipse fluorescence spectrophotometer equipped with a Xenon flash lamp (Agilent), according to a protocol modified from previous studies.[9] Based on optimization of peptide concentration and incubation time for the absorbance spectroscopy assay described above, solubilized peptide (6mM) was incubated with 0.25μM RHO samples on ice for 10 min then transferred to cuvettes. Fluorescence measurements were recorded at 30-s intervals with a 2 s integration time, using an excitation wavelength of 295 nm (1.5 nm slit width) and an emission wavelength of 330 nm (10 nm slit width). There was no noticeable activation by the excitation beam prior to RHO activation. RHO samples were bleached for 30 s at 20°C with a fiber optic lamp (Dolan-Jenner) using a filter to restrict wavelengths of light below 475 nm to minimize heat. Following the fluorescence plateau approximately 70 min after light bleaching ((F_{MAX}), indicating an equilibrium between ATR release and re-uptake, 5mM hydroxylamine (NH_2OH) was added to push the equilibrium towards complete ATR release from the MII binding pocket by converting ATR to ATR-oxime which can no longer fit into the binding pocket), as previously described (Figure S3).[9] The spike in fluorescence after NH_2OH addition was calculated as % maximum fluorescence using the equation (F_{max} after NH_2OHaddition – F_{max} before NH_2OHaddition)/ F_{max} after NH_2OHaddition) (Data S1B and S1C).[47] Therefore, % maximum fluorescence indicates the amount of ATR trapped in MII binding pocket, and thus represents the amount of extra MII formed after photoactivation.[47] The relative extra MII formation was calculated by normalizing the % maximum fluorescence to no-peptide control. In line with these studies, we demonstrated that titration with exogenous all-trans-retinal shifts the equilibrium towards all-trans-retinal rebinding by MII, resulting in incomplete retinal release (Figure S3; Data S1B and S1C). By stabilizing the MII confirmation, GtαCT-HA and Arr-1-FL peptide binding can also shift this equilibrium towards all-trans-retinal rebinding, which we also observed for the GtαCT-HA peptide (Figure S3), consistent with previous reports.[9] A recent study shows that the orientation of the finger loop in full-length arrestin is similar to that of the Arr1-FL peptide,[72] consistent with previous studies.[44,45] For full-length Arr-1, stabilization of MII normally requires activation via phosphorylation of the RHO C-terminus, as well as the addition of negatively charged phospholipids to detergent micelles to recapitulate physiological interactions between the positively charged Arr-1 C-edge loop membrane anchor and the rod disc membrane[47,73] Importantly however, the Arr-1-FL peptides are capable of bypassing both requirements for RHO binding.[16,17,45] Consistent with this, using fluorescence spectroscopy we found that Arr-1-FL peptides can cause incomplete decay of MII in detergent micelles without RHO phosphorylation nor the addition of negatively charged phospholipids (Figure 3A). These results reproduce that of previous studies described above, altogether validating that within detergent micelles, Arr-1-FL peptides can promote all-trans-retinal rebinding in a manner functionally similar to full-length Arr-1.

Crystal structure modeling

The two amino acid substitutions were modelled onto the crystal structure of human RHO bound to mouse arrestin PDB:4ZWJ [15] and the distances from the two residues to the RHO were measured using UCSF Chimera.[74] The substitutions of interest, Q69R and S78K, both involve a drastic change in size, orientation and charge of the amino acid side chain which can have implications on the binding interaction of arrestin to RHO. The residues at the two sites change from polar uncharged to positively charged side chain, as well as an extension in length of the side chain. Structural modeling of the mutations in the crystal structure of arrestin bound to active MII RHO (PDB:4ZWJ) reveal an increased proximity of the residues towards RHO (Figure S4). The deep-diving whale and owl

identity, R69, is orientated towards the RHO binding interface which closes the distance to T70 of RHO (Figure S4). Moreover, it extends within 5.0Å in proximity of P71, which is not the case for the bovine identity, Q69. Similarly, K78 is approximately half the distance to V139 of RHO than S78 (Figure S4). The proximity of these additional interactions, as well as the change in electrostatic properties may facilitate stronger binding of arrestins in dim-light adapted animal (owls, minke and sperm whales) in comparison to diurnal animals such as the bovine model organism.

QUANTIFICATION AND STATISTICAL ANALYSIS

For analyses of molecular evolutionary rates (PAML), likelihood ratio tests of alternative vs. null models were used to determine statistical significance against a X^2 distribution.[69] The best fitting model for each dataset was assessed by differences in AIC. For fluorescence spectroscopy analyses of incomplete MII decay, significant differences in peptide effects were calculated using a two-sided t-test. N = 3 biological replicates (independent experiments using independent RHO purifications) were used.